Available online at www.sciencedirect.com
SCIENCE DIRECT®
Catalysis Today 85 (2003) 101–111
CATALYSIS TODAY
www.elsevier.com/locate/cattod

# Using scanning tunneling microscopy to characterize adsorbates and reactive intermediates on transition metal oxide surfaces

E. I. Altman [a,*], R. E. Tanner [b]

[a] *Department of Chemical Engineering, Yale University, New Haven, CT 06520, USA*
[b] *Department of Physics, University of Warwick, Coventry CV4 7AL, UK*

Received 7 February 2003; received in revised form 12 April 2003; accepted 13 April 2003

**Abstract**

Scanning tunneling microscopy (STM) is demonstrated to be a powerful tool to characterize adsorption and reaction on oxide surfaces by imaging molecular adsorbates and reactive intermediates. The molecules were used to probe surface structure and to study surface reactivity spatially at the atomic level. Results for three systems are presented: alcohol adsorption on $WO_3$(0 0 1), carboxylates on the anatase polymorph of $TiO_2$, and propene adsorption on a PdO monolayer on Pd(1 0 0). When the alcohols were exposed to the $WO_3$(0 0 1)-c(2 × 2) surface at room temperature the molecules could not be imaged. Heating the surface to temperatures above a water desorption peak associated with alcohol deprotonation, however, allowed 1-propoxide to be imaged. The images reveal that the alkoxide has no preference for defects, rather it binds to $W^{6+}$ ions exposed on the fully oxidized c(2 × 2) surface. Temperature-programmed desorption revealed that alkoxides at these sites undergo only dehydration reactions. To probe the structure of the unusual (1 × 4) reconstruction on anatase (0 0 1), formic and acetic acid adsorption were used. Following dissociative adsorption, both formate and acetate adsorb solely centered atop the bright rows that define the surface reconstruction, and the molecules are always at least two lattice constants apart. This result may be attributed to carboxylates bridge-bonded to Ti atoms at the center of the bright rows. This finding eliminates several suggested models of the reconstruction and suggests that a recently proposed ad-molecule model is a good representation of the surface structure. Propene was observed to initially randomly adsorb on the PdO monolayer. At higher coverages, however, the adsorbates cluster, disrupting the surface structure and causing the adsorption rate adjacent to the clusters to increase. Temperature-programmed reaction revealed that once propene adsorbs, the oxide monolayer catalyzes its oxidation at lower temperatures than metallic Pd, but that the propene sticking coefficient on the ordered oxide layer is a factor of 5 lower.


*Keywords:* STM; Oxide; Anatase; Tungsten oxide; Palladium; Adsorption

## 1. Introduction

Since the development of scanning tunneling microscopy (STM), the ability to image surfaces with atomic or molecular resolution has been recognized as a boon to understanding basic processes on surfaces including catalysis. In addition to imaging, measuring the tunnel current as a function of the tip–sample bias voltage yields spectra that are related to the local electronic density of states (DOS) within a few electron volts of the Fermi level, providing insight into how molecules bond to surfaces. More recently, it has been demonstrated that the energies of the vibrational transitions of individual adsorbates can be extracted

* Corresponding author. Tel.: +1-203-4324375; fax: +1-203-4324387.
*E-mail address:* eric.altman@yale.edu (E.I. Altman).

0920-5861/$ – see front matter © 2003 Elsevier B.V. All rights reserved.
doi:10.1016/S0920-5861(03)00379-1

from tunneling spectra recorded at cryogenic temperatures [1]. Finally, unlike most other surface science techniques, STM does not require ultra-high vacuum (UHV) and so there need not be a "pressure gap" between STM and catalytic experiments.

There are, however, challenges to applying STM to problems of interest in catalysis. STM images reflect contours of constant integrated local DOS that do not necessarily coincide with atomic positions. Therefore, reactive intermediates cannot always be identified simply by looking at STM images. One approach to surmount this problem has been to compare calculated images of candidate molecules with the experimental data [2]. Another challenge with the transition metal surfaces of interest to catalysis, such as Pt and Pd, is the delocalized nature of adsorbate bonding, which results in molecules that move across the surface at rates greatly exceeding the imaging rate. This problem has been overcome by freezing-out the diffusional motion using low temperatures or by locking the molecules in place using high coverages [3,4]. The disadvantage of these approaches is the possible shift away from the temperature or coverage regimes of interest in catalysis.

Some of the difficulties associated with imaging molecules on metal surfaces are less severe on transition metal oxides. In particular, the localized bonding on oxide surfaces suggests that diffusion barriers on these surfaces should be high enough to allow imaging of isolated adsorbates at room temperature and above. The information gained by imaging adsorbates on oxides is also potentially more interesting because defects are often invoked to explain reactivity: a problem ideally suited to the real space imaging capabilities of STM.

Until recently there has not been a great deal of work done on imaging adsorbates on transition metal oxides. The most detailed studies have been on carboxylates on the rutile phase of $TiO_2$, where the adsorption site, molecular orientation, diffusion mechanism, and diffusion rate have all been characterized [5–10]. In this paper we describe our recent efforts on characterizing adsorbates and reactive intermediates on oxide surfaces with STM in conjunction with macroscopic surface characterization techniques, particularly temperature-programmed desorption (TPD) and temperature-programmed reaction (TPR). Three systems will be discussed: alkoxides on $WO_3$(0 0 1); carboxylates on the anatase polymorph of $TiO_2$; and propene on a PdO(0 0 1) monolayer on Pd(1 0 0). Each system demonstrates a different type of problem in catalysis and surface science that can be addressed using STM, while all illustrate how combining an atomic scale view of the surface with macroscopic reactivity measurements yields a direct, detailed picture of the connection between structure and activity and selectivity.

## 2. Experimental

Experiments were performed using an UHV system equipped with a double pass cylindrical mirror analyzer for Auger electron spectroscopy (AES), low-energy electron diffraction (LEED) optics, a quadrupole mass spectrometer, an ion gun, and a high-speed variable-temperature scanning tunneling microscope [11]. The main UHV chamber is connected to a side chamber in which samples can be heated up to 900 K at pressures up to the Torr range. The base pressure of the main chamber is in the high range of $10^{-11}$ Torr.

Single crystal samples were used in the $WO_3$ experiments. The crystals were cleaved in air to expose the (0 0 1) surface. Clean stoichiometric surfaces were prepared by annealing at 775–885 K in $3 \times 10^{-5}$ Torr of $O_2$ for more than 10 h. Following this procedure, AES spectra revealed no detectable impurities and clear LEED patterns with low diffuse backgrounds were obtained.

Epitaxial (0 0 1)-oriented thin $TiO_2$ films on conductive Nb-doped $SrTiO_3$(1 0 0) were used for anatase experiments. The films were grown by physical vapor deposition in an oxygen plasma at the Pacific Northwest National Laboratory (PNNL). At Yale, the anatase surfaces were subsequently prepared by 500 eV $Ar^+$ bombardment to remove carbonaceous deposits followed by annealing at 1025 K in $O_2$. This procedure yielded clean stoichiometric anatase surfaces with sharp $(1 \times 4)$ LEED patterns.

The PdO monolayer was prepared by exposing $NO_2$ to a clean Pd(1 0 0) surface at 500–600 K. At these temperatures $NO_2$ rapidly dissociates on Pd creating O atoms that stay on the surface and NO that rapidly desorbs [12]. Above $NO_2$ exposures greater than ~20 L, STM images showed that the surface was completely covered by a $(\sqrt{5} \times \sqrt{5})R27^\circ$ structure that has

been attributed to an epitaxial PdO(0 0 1) monolayer [13].

Electrochemically etched W tips were used in all STM experiments. The tips were cleaned by electron beam bombardment prior to use. Although the molecules of interest adsorb and dissociate on W, no artifacts due to adsorption on the tip were observed even with more reactive species such as $NO_2$, $Br_2$, and $Cl_2$ [14,15]. All the images were recorded at tunnel currents between 0.1 and 1.0 nA.

## 3. Results and discussion

### 3.1. Alkoxides on $WO_3$(0 0 1)

As illustrated in Fig. 1(a), the $WO_3$ structure can be approximated as a cubic network of corner-sharing octahedra. Viewed down the [0 0 1] direction, $WO_2^{2+}$ planes alternate with $O^{2-}$ planes; terminating the crystal in either plane would yield a high-energy polar surface. To avoid this, a non-polar surface is created by terminating the crystal with a half plane of O atoms. In the simplest arrangement, the oxygen atoms cover every other W ion in the underlying $WO_2$ plane, resulting in the c(2 × 2) structure pictured in Fig. 1(b) [16]. While this surface can be viewed as missing oxygen, all the W ions are in the +6 oxidation state and so no additional oxygen can be adsorbed without requiring the W ions to adopt unphysical oxidation states. Thus the c(2 × 2) surface is considered fully oxidized.

In terms of catalytic chemistry, interesting questions surrounding the c(2 × 2) surface include:

- whether exposing a W ion is sufficient for adsorption and reaction;
- if exposed $W^{6+}$ ions are active, which catalytic pathways they favor;
- whether the pathways change as the ions are reduced.

We have been addressing these questions by studying the adsorption and reaction of a series of alcohols using TPD and characterizing the adsorption sites with STM [17,18]. The alcohols were selected because they may undergo either dehydration to yield olefins or dehydrogenation to yield aldehydes and ketones; thus in addition to providing kinetics the TPD results reveal the surface's relative activity for these two oxidation pathways. Primary, secondary and tertiary alcohols were compared to determine if the pathway changes as the molecules become easier to dehydrate. For all the molecules studied, only dehydration products were found in TPD from c(2 × 2) surfaces [19]. The alkenes desorbed in reaction-limited desorption peaks whose peak temperatures shifted to lower temperature downward through the series 1-propanol, 2-propanol, *t*-butanol. The downward shift as the molecules became easier to dehydrate suggests that breaking the C–O bond is the rate-limiting step.

As shown in the empty-states STM image in Fig. 2(a), a $WO_3$ surface that gives an intense c(2 × 2) LEED pattern still exhibits numerous defects

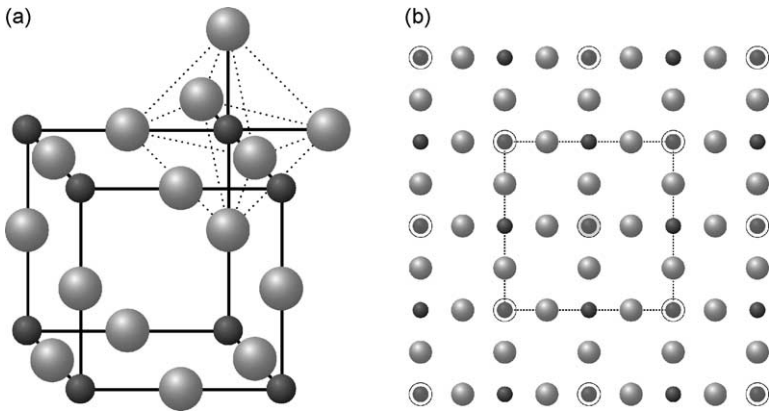


Fig. 1. (a) Cubic approximation of the $WO_3$ structure. The solid lines highlight the unit cell and the dashed lines indicate a $WO_6$ octahedron. (b) Model of the $WO_3$(0 0 1)-c(2 × 2) surface. The dashed line highlights the c(2 × 2) unit cell. Small dark balls represent W atoms and large lighter balls O atoms; in (b) the outermost O atoms are shown as partially transparent and are outlined in black.

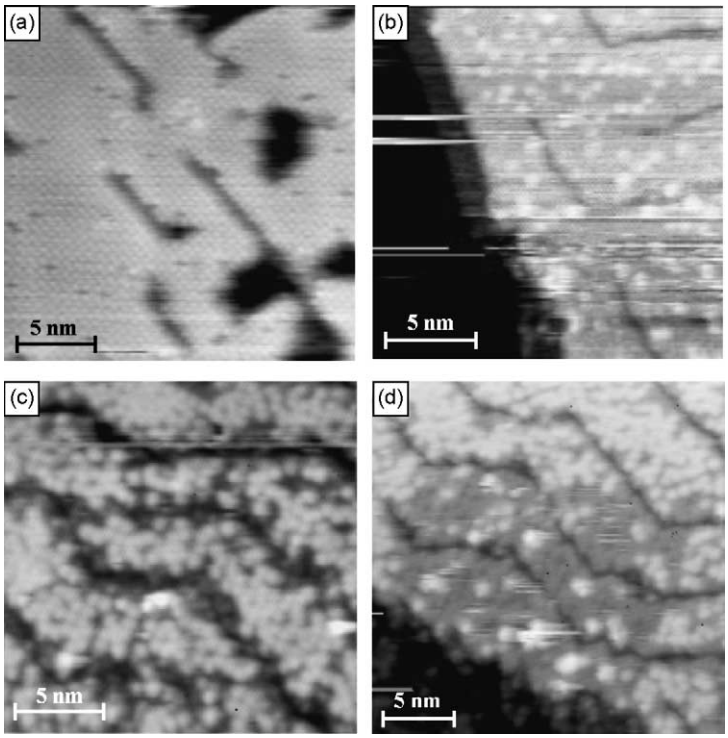


Fig. 2. (a) STM image of a clean $WO_3$(0 0 1)-c(2 × 2) surface obtained at a sample bias voltage of 2.0 V. (b) Image with bias voltage of 1.5 V obtained after exposure to 30 L of 1-propanol at room temperature and then brief annealing at 400 K. (c) Image following exposure to 90 L of 1-propanol and annealing at 400 K, recorded at 2.0 V. (d) Image of 1-propoxide on $WO_3$(0 0 1) recorded at 2.0 V after repeatedly scanning the central area at 1.25–1.5 V.

including steps, line defects, and vacancies. Although empty-states STM images of many transition metal oxides reveal the positions of the metal atoms, the O atoms in the c(2 × 2) structure are raised so far above the $WO_2$ plane (∼0.19 nm) that the image contrast is dominated by topography rather than variations in the local DOS. The periodic bright dots therefore correspond to terminal oxygen atoms [16] and the small dark features to oxygen vacancies. The presence of the defects means that the TPD results alone are insufficient to attribute the observed dehydration activity to $W^{6+}$ ions in c(2 × 2) terraces, and so we turned to STM to image the alcohols (or reactive intermediates originating from the alcohols) on the surface.

When the $WO_3$ surfaces are exposed to alcohols at room temperature, STM images show no apparent change in the surface. In the TPD experiments, water and unreacted alcohol are observed to desorb in broad peaks at 425 K, prior to alkene desorption [19]. The simultaneous desorption of water and unreacted alcohol suggest that the water desorption is due to deprotonation of the remaining alcohol to form a more strongly bound alkoxide. In subsequent STM experiments the surface was exposed to alcohol at room temperature and then heated to 400 K before imaging. The primary alcohol, 1-propanol, was chosen because it exhibits the greatest separation between the lower temperature water desorption peak and the higher temperature alkene peak, making it the easiest alcohol to deprotonate without undergoing further reaction. Fig. 2(b) shows the surface following a 30 L dose of 1-propanol. The most obvious new features are the white or raised dots randomly distributed on the terraces. When the 1-propanol exposure was increased to 90 L (Fig. 2(c)), the surface became covered by a higher density of the bright features. The correlation of dose and density allowed us to attribute the bright features to 1-propoxide. The images also show that

1-propoxide has no particular affinity for either steps or line defects. Since the vacancy density on the terraces is insufficient to account for the density of features in Fig. 2(c), we conclude that defects do not play a strong role in the reactivity of the c(2 × 2) surface. In images similar to Fig. 2(b), the c(2 × 2) structure of the substrate could be resolved simultaneously with the adsorbates. Superimposing a grid on the images revealed that the adsorbates are located between the O atoms in the c(2 × 2) structure, and on top of the W atoms, as would be expected.

Imaging the alkoxide required high sample bias voltages, greater than ∼1.5 V with the exact value dependent on the tip. When the bias voltage was reduced below this level, the molecules were swept aside by the tip as illustrated in Fig. 2(d). In this case, the central square region was imaged repeatedly at 1.25–1.5 V before the bias voltage was set to 2.0 V and the wider range image in the figure was recorded. The image shows a severely denuded square area where the tip was scanned at the lower bias. Zooming in on the denuded area revealed the c(2 × 2) structure. Reducing the bias favored sweeping the molecules aside because lower biases require smaller tip–surface separations to obtain the same tunneling current, and therefore tip–adsorbate interactions are stronger at lower biases. Thus STM can be used to image an adsorbate, remove it, and then image the structure of the underlying site. This unique capability of scanning probe techniques will be particularly important for surfaces where the reactivity is dominated by a minority of defect sites.

Together the STM and TPD results indicate that the $WO_3$(0 0 1)-c(2 × 2) surface is active for alcohol dehydration but not dehydrogenation, that the active sites are exposed to $W^{6+}$ cations, and that surface defects do not greatly affect the reactivity.

### 3.2. Carboxylates on anatase(0 0 1)

There have been a great number of surface science studies on the rutile phase of $TiO_2$ but few on anatase, the phase most often used in catalysis. This stems primarily from the availability of large rutile single crystals rather than greater inherent interest in the rutile phase. Recently, however, several groups have been able to grow epitaxial anatase thin films [20–23]. Studies of these films have shown that the anatase (0 0 1) surface undergoes an unusual (1 × 4) reconstruction [20,24]. Unlike $WO_3$(0 0 1), bulk-terminated anatase (0 0 1) is non-polar, and so the reconstruction is not driven by the need to create an autocompensated surface. While several models of the reconstruction have been proposed [20,24,25], all have weaknesses or uncertainties and so the structure has remained an open question. A great deal is known about carboxylates on other $TiO_2$ surfaces including how they prefer to bond, what they look like in STM images, and how their reaction pathways depend on the coordination of the surface Ti atoms [5–8,26–29]. The lowest coordinated sites should be the most reactive, thus the molecules can be used as structural probes of coordination. We have characterized acetate and formate chemistry on anatase (0 0 1)-(1 × 4) using TPD, and imaged the location of the adsorbates with STM and non-contact atomic force microscopy (NC-AFM) [18,30]. From this data structural models of the reconstruction were evaluated.

As shown in Fig. 3(a), the bare (1 × 4) surface is defined by bright rows ∼0.1 nm high separated by slightly less than 1.6 nm, which corresponds to four times the lattice constant. Fig. 3(b) and (c) shows the surface after exposure to formic and acetic acids near room temperature. On adsorption the acids deprotonate to form formate and acetate. The images show that both types of molecules adsorb solely atop the bright rows of the reconstruction and tend to appear as ovals, elongated perpendicular to the bright rows. The molecules always appear centered on the bright row and are never closer than two anatase lattice spacings apart. As shown in Fig. 3(d), the resolution improves dramatically when the formate-covered surface is flashed to 850 K.

TPD results for well-ordered (1 × 4) surfaces reveal only decomposition products at high temperatures, above 750 K [18]. On the other hand, surfaces that contain defects behave differently. After bombarding the surface with 500 eV $Ar^+$ ions and annealing at 575 K, STM images show that the bright rows are frequently interrupted by defects including anti-phase domain boundaries [18]. When such surfaces are exposed to formic and acetic acid, additional products desorbed from the surface, primarily those associated with dehydration. Thus molecules adsorbed on the (1 × 4) terraces decompose at high temperatures. Significantly, no bimolecular coupling products such as acetone from acetate were ever seen.

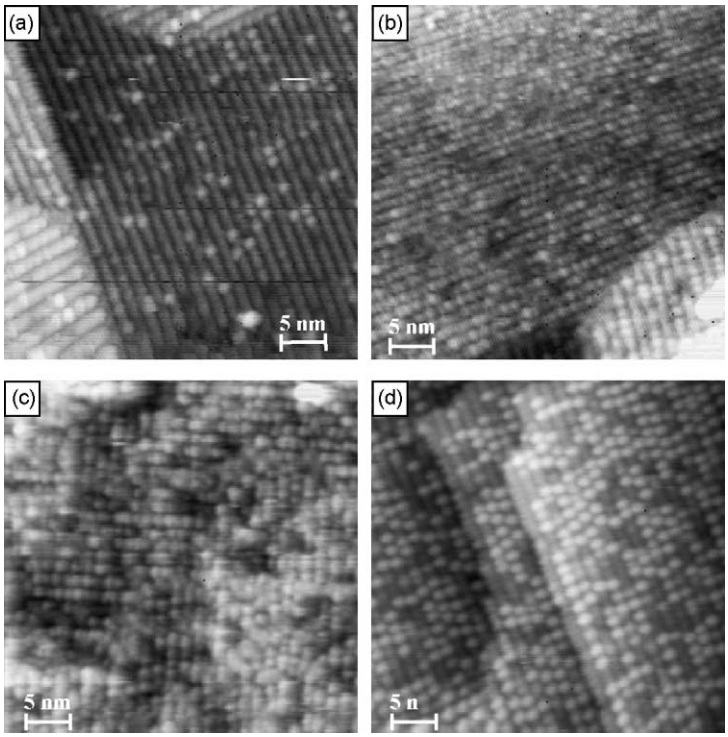


Fig. 3. (a) STM image of the (1 × 4) reconstructed anatase (0 0 1) surface recorded at a sample bias of 1.5 V. (b) Image recorded at 3.5 V after exposure of the anatase surface to formic acid at room temperature. (c) Image of an acetate-covered anatase surface formed by acetic acid exposure at room temperature, recorded at 1.1 V. (d) After flashing the formate-covered surface to 850 K, this image recorded at 2.5 V shows that the resolution dramatically improved.

On rutile (1 1 0), formate and acetate bridge bond to neighboring exposed fivefold coordinated $Ti^{4+}$ ions [8]. In empty-states STM images the molecules appear elongated perpendicular to the plane of the molecule. This has been attributed to the images being dominated by tunneling into the lowest unoccupied molecular orbital (LUMO) of the carboxylates, which is oriented perpendicular to the plane of the molecule [8]. The similar shape in the images of carboxylates on anatase (Fig. 3) as well as the minimum 2× separation indicates that the carboxylates bond to the reconstructed anatase surface in a similar way. With molecules centered along the bright rows, the images indicate that Ti atoms are exposed in the middle of the bright rows. Work on rutile surfaces suggests that bimolecular ketonization reactions require bonding of the two ligands to a common surface $Ti^{4+}$ cation [28]. The lack of bimolecular products for the anatase surface means that the Ti atoms on the bright rows have only one accessible vacant coordination site.

It has been suggested that the (1 × 4) reconstruction is due to microfaceting. Three models have been proposed: one exposing {1 0 3} facets [24], another {1 0 4} facets [20], and a third {1 0 1} facets [18]. None of these models is consistent with all of the data. The {1 0 3} microfacet model has pairs of fourfold coordinated Ti atoms straddling either side of the bright row. The {1 0 4} model has Ti atoms centered atop the bright row; however, it also exposes fourfold Ti in the trenches where preferential adsorption was not observed. The {1 0 1} model is appealing in that it exposes fivefold coordinated Ti atop the middle of the bright row and because the {1 0 1} facets it exposes are believed to be the lowest surface energy planes in anatase [31]. The model, however, suggests corrugations of at least 0.4 nm, far in excess of the observed ∼0.1 nm. Added and missing row models have also

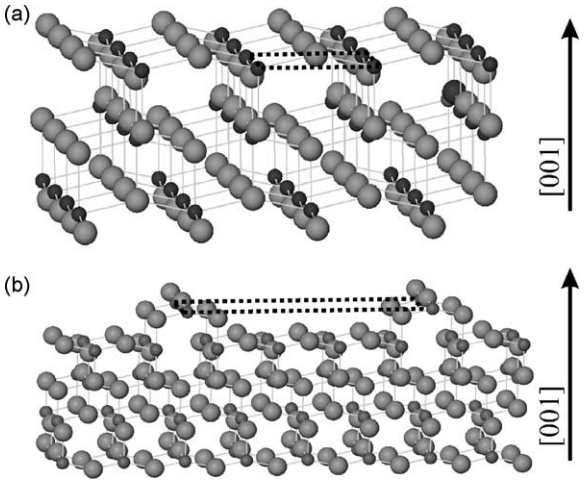


Fig. 4. Illustrations showing: (a) the bulk-terminated anatase (0 0 1) surface and (b) the ad-molecule model proposed for the (1 × 4) reconstruction of anatase (0 0 1) by Lazzeri and Selloni [32]. In the figure, small, dark balls represent Ti atoms and large lighter balls O atoms. The dashed lines highlight the surface unit cell. The illustration in (b) does not include the relaxation of the surface atoms away from their bulk positions predicted by Lazzeri and Selloni.

been suggested that are not stoichiometric, but this is not consistent with XPS data that show that the reconstructed surface is fully oxidized [20].

The model that best explains the experimental results is the ad-molecule model proposed by Lazzeri and Selloni [32] and pictured in Fig. 4. In this model, a row of oxygen atoms is replaced by an added $TiO_3$ row. The resulting surface is stoichiometric with a corrugation of ∼0.15 nm, consistent with XPS and STM results. Titanium atoms are centered along the raised rows, which is consistent with the location of the carboxylates. Although the Ti atoms on the rows are only fourfold coordinated, one of the vacant coordination sites is inaccessible because it projects downwards towards the bulk, so these Ti atoms would not be expected to be capable of catalyzing bimolecular coupling reactions, as our TPD experiments demonstrated.

Typically in catalysis we are interested in how surface structure affects reactivity. In this example, we have turned the usual problem around. We have used well-characterized chemical probes to help determine the structure of a complex surface. By characterizing both the surface chemistry and the location of the adsorbates, we have eliminated several structural models and shown that the ad-molecule model can explain all of the available experimental data.

### 3.3. Propene adsorption and reaction on a PdO(0 0 1) monolayer

Palladium is the most promising catalyst for the complete oxidation of hydrocarbons in catalytic combustors [33]. Under reaction conditions, Pd can change from the metallic to the oxidic form and transitions between these states cause the catalyst activity to change. In the catalysis literature it has been suggested that the oxide phase is more active below ∼1000 K while surface science studies have shown that oxygen blocks sites for hydrocarbon adsorption and dissociation [33–35]. We have sought to address this contradiction by studying how oxidation reactions on Pd surfaces depend on oxygen coverage, from the oxygen chemisorption regime to the regime where bulk PdO forms on the surface [36–38].

As the oxygen coverage is increased on Pd(1 0 0), a series of ordered phases form culminating in a $(\sqrt{5} \times \sqrt{5})R27^\circ$ structure [37,39,40]. Tensor LEED studies have shown that the $(\sqrt{5} \times \sqrt{5})R27^\circ$ pattern is well explained by an epitaxial monolayer of PdO(0 0 1) [13]. Fig. 5(a) illustrates the structural relationship between the PdO monolayer and the underlying metal. TPD experiments at Yale have revealed an $O_2$ desorption peak slightly above that anticipated for PdO dissociation suggesting that the Pd–O bond in the monolayer is slightly stronger than in bulk PdO [37]. In STM images of the PdO monolayer (Fig. 5(b)), the bright dots are separated by 0.61 nm or $\sqrt{5}$ times the Pd(1 0 0) spacing. This is consistent with the tensor LEED study, which showed that the predominant corrugation in the surface is due to the PdO layer coming into and out of registry with the substrate [13]. In Fig. 5(b) the resolution appears to be better in one direction than the other, almost leading to a striped appearance. While such an appearance is usually attributed to a tip artifact, that is not the case here. Fig. 5(c) shows multiple domains of the $(\sqrt{5} \times \sqrt{5})R27^\circ$ structure with the stripes rotated by 90° in the same image. (The black and white lines at the step edge are a consequence of contrast enhancement on different terraces.) Figure 5(a) shows how the PdO(0 0 1) surface contains rows of Pd atoms connected by bridging oxygen along PdO[0 1 0] but not along PdO[1 0 0]. The striped appearance can be

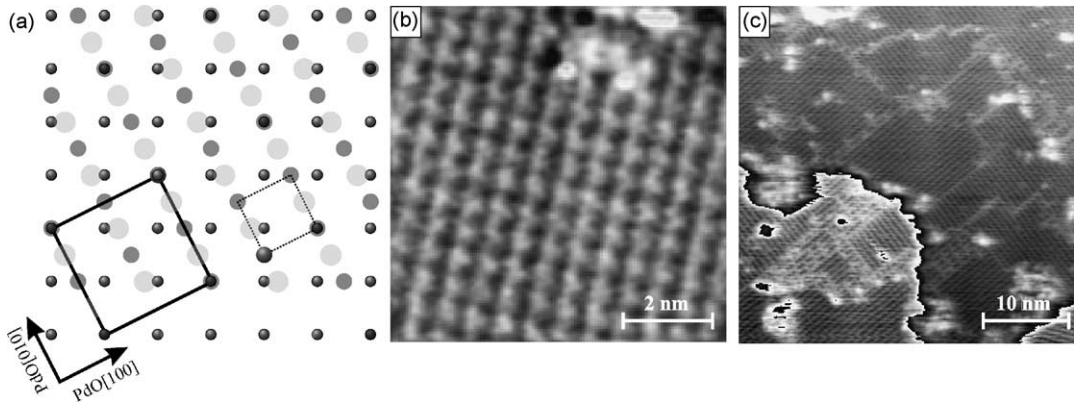


Fig. 5. (a) Structural model of an epitaxial PdO monolayer on Pd(1 0 0). The smallest dark balls represent Pd atoms in Pd(1 0 0), while the small partially transparent circles represent Pd atoms in PdO and the larger circles the O atoms. The solid square highlights the $(\sqrt{5} \times \sqrt{5})R27^\circ$ surface unit cell and the dashed square the PdO(0 0 1) unit cell. (b) High resolution STM image of the $(\sqrt{5} \times \sqrt{5})R27^\circ$ structure recorded at 1.25 V. (c) Wider range STM image recorded at 1.5 V showing multiple domains of the $(\sqrt{5} \times \sqrt{5})R27^\circ$ structure. To enable the atomic structure to be resolved on both terraces, the contrast was enhanced by cycling through the grayscale twice.

attributed to the inequivalence of the two directions [37].

Fig. 6 shows TPR curves for propene exposure to the PdO monolayer: (a) shows the $CO_2$ formed, (b) the $H_2O$, and (c) the desorption of any remaining oxygen. At the lower propene dose (0.5 L) $CO_2$ desorbs at 430 K, while for the higher propene dose (5 L) a second $CO_2$ peak appears at 550 K. At the lower dose it was difficult to detect the water formed by the reaction, but at 5 L it is clear that the water desorbs simultaneously with the lower temperature $CO_2$ peak. For propene doses below 10 L, the mass spectrometer signal at 28 amu perfectly tracked the $CO_2$ peak but the intensity was much lower, in the range expected for $CO_2$ cracking. Above 10 L, however, all of the oxygen was consumed by the reaction and the peak

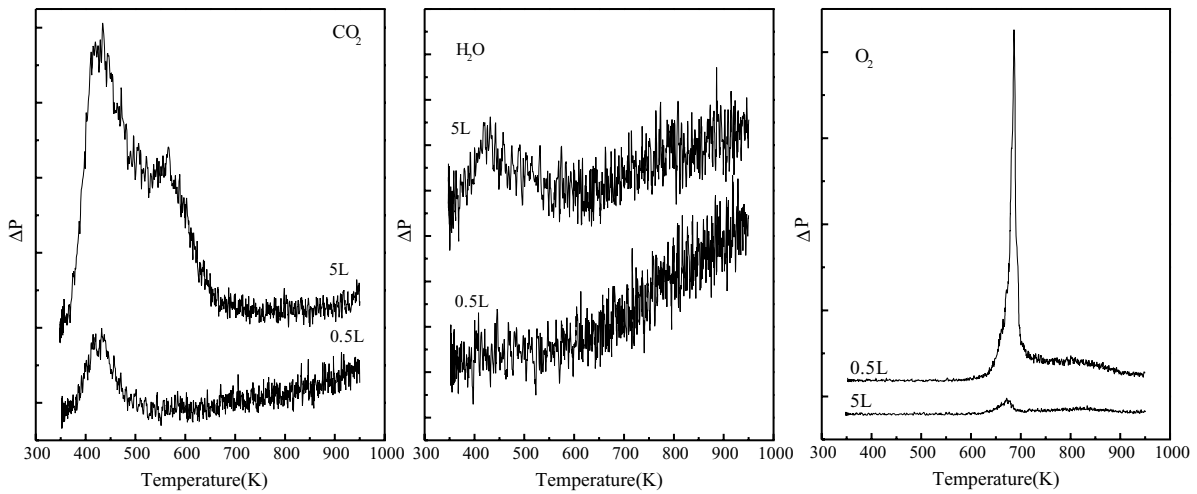


Fig. 6. TPR curves for propene exposure to Pd(1 0 0) surfaces pre-exposed to 45 L $NO_2$ at 500 K which led to sharp $(\sqrt{5} \times \sqrt{5})R27^\circ$ patterns. During each run $CO_2$, $O_2$, $H_2O$, and CO were monitored along with several other species. For the propene doses shown in the figure only $CO_2$, $O_2$, and $H_2O$ desorption were detected. A heating rate of 5 K $s^{-1}$ was used.

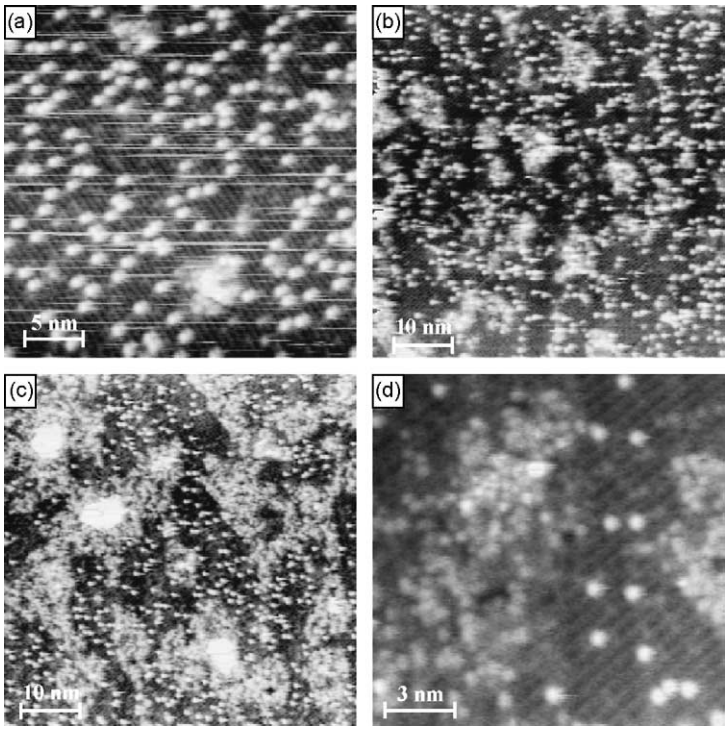


Fig. 7. (a) STM image obtained following room temperature in situ propene exposure to a PdO monolayer on Pd(1 0 0). (b) A wider range view of the surface illustrated in (a) reveals disordered regions in addition to the bright dots distributed across the surface. (c) After increasing the propene exposure, the disordered areas cover more of the surface. (d) Zooming in on (c) reveals the surface unit cell of the $(\sqrt{5} \times \sqrt{5})R27^\circ$ regions and shows that the disordered regions are made up of similar bright dots. The images were recorded at sample biases between 1.0 and 2.5 V, over this range the appearance of the images did not depend strongly on the bias voltage.

intensity at 28 amu exceeded the $CO_2$ peak intensity signaling a shift to CO formation and incomplete combustion. The CO desorbed at 430 K. The experiments also revealed that the propene sticking coefficient increases with propene exposure. When propene is exposed to a Pd(1 0 0) surface with chemisorbed oxygen, the 550 K $CO_2$ peak is seen with only a very weak low temperature shoulder, and the initial sticking coefficient is a factor of 5 greater.

Fig. 7 shows a series of STM images for increasing propene exposure at room temperature. The stripes in the images are due to the $(\sqrt{5} \times \sqrt{5})R27^\circ$ structure. At the lowest dose, Fig. 7(a) shows bright dots randomly distributed across the terrace. Their density increases with exposure, so the bright dots can be attributed to adsorbed propene or fragments originating from propene. At room temperature, there is no evidence of water production when propene is exposed to the surface, suggesting that the molecules adsorb largely intact. Fig. 7(b) shows the surface on a larger scale. Here it is evident that there are amorphous regions in addition to the bright dots. When the coverage is increased (Fig. 7(c)), the amorphous areas grow while comparatively few bright dots are added to the $(\sqrt{5} \times \sqrt{5})R27^\circ$ ordered areas. The higher resolution image in Fig. 7(d) shows that the disordered areas are made up of discrete dots similar to the isolated dots seen on the ordered terraces. STM movies recorded during propene exposure showed that the disordered areas are due to clustering of adsorbates that lead to a higher adsorption rate at the edges of the clusters, and explain the observed increase in propene sticking coefficient with exposure.

The results indicate that the ordered PdO monolayer has a much lower sticking coefficient for hydrocarbons than does metallic Pd covered by chemisorbed oxygen, but that once hydrocarbon molecules adsorb oxidation is more facile on the oxide surface.

The relative magnitude of these two effects will determine if the oxide or the metal is more active. The STM results show that propene adsorption disrupts the surface structure causing the sticking coefficient to increase. While this also causes a higher temperature reaction peak to appear, the lower temperature peak persists, indicating that disrupting the oxide surface structure does not turn off the lower activation energy pathway. Rather, the higher temperature peak is attributed to reaction at 430 K removing oxygen from the surface causing a transition back to chemisorbed oxygen on metallic Pd. The chemisorbed oxygen then reacts with any remaining propene or propene fragments at 550 K. This is supported by the observation that the high temperature pathway shuts down first when the propene coverage is so high that there is not enough oxygen to complete the reaction. Thus the STM and TPR results together suggest that by disrupting or otherwise modifying the oxide surface structure it may be possible to take advantage of the more facile surface reaction step on the oxide without suffering from a low reaction probability.

## 4. Summary

Imaging molecular adsorbates and reactive intermediates with STM in conjunction with macroscopic surface characterization can provide a uniquely detailed view of catalytic reactions on oxide surfaces. Three examples were presented: alcohol adsorption on tungsten oxide, carboxylic acids on the anatase polymorph of $TiO_2$, and propene adsorption on an epitaxial PdO surface layer on Pd(1 0 0). The results indicate that alcohols molecularly adsorb on $WO_3$(0 0 1)-c(2 × 2) at room temperature, but the rapid motion of the intact molecules makes them impossible to image at 300 K. Annealing to deprotonate the alcohol yields strongly localized alkoxides such as 1-propoxide that can be readily imaged. The alkoxides bond to W atoms exposed on c(2 × 2) terraces with no particular affinity for defects. These c(2 × 2) sites are active for alcohol dehydration but not dehydrogenation.

Anatase (0 0 1) exhibits an unusual (1 × 4) surface reconstruction. Well-characterized carboxylate chemistry was used to gain insight into the structure of the reconstructed surface. Both formate and acetate adsorb centered atop the bright rows that define the reconstruction. Further, the surface is not active for bimolecular ketonization reactions associated with Ti atoms exposing more than one vacant coordination site. These findings rule out microfacet models of the reconstruction that place fourfold coordinated Ti in the troughs or straddling either side of the bright row, but are consistent with the recently proposed ad-molecule model.

The results for the PdO monolayer help explain how Pd oxide can be more active for hydrocarbon oxidation than metallic Pd. Once hydrocarbons adsorb on the oxide layer, subsequent oxidation is more facile on the oxide than on the metal. The adsorption probability on the oxide, however, is much lower. Initial adsorption on the oxide layer is slow but as the coverage increases clusters of molecules form that disrupt the surface structure and at the periphery of the clusters the adsorption is enhanced. Disrupting the surface structure does not shut down the lower temperature oxidation pathway, suggesting that by controlling the oxide surface structure both a high adsorption probability and a facile surface reaction step can be achieved.

## Acknowledgements

The authors wish to thank R.G. Egdell for the $WO_3$ crystals, Y. Liang for the anatase thin films, and A. Sasahara and H. Onishi for their collaboration on NC-AFM of anatase. The assistance of M. Li, G. Zheng, P. Meethunkij, L.H. Chan, and W. Gao is also appreciated. This work was supported by the US Department of Energy through Basic Energy Sciences grant no. DE-FG02-98ER14882 and the Petroleum Research Foundation through grant no. ACS-PRF-34181-AC5.

## References

[1] B. C. Stipe, M. A. Rezaei, W. Ho, Science 280 (1998) 1732.
[2] D. N. Futaba, J. P. Landry, A. Loui, S. Chiang, Phys. Rev. B 65 (2002) 0451061.
[3] P. S. Weiss, D. M. Eigler, Phys. Rev. Lett. 71 (1995) 3139.
[4] P. Sprunger, F. Besenbacher, I. Stensgaard, Surf. Sci. 324 (1995) L321.
[5] H. Onishi, K. I. Fukui, Y. Iwasawa, Colloid Surf. A 109 (1996) 335.

[6] H. Onishi, K. I. Fukui, Y. Iwasawa, Jpn. J. Appl. Phys., Part 1 38 (1999) 3830.
[7] H. Onishi, Y. Iwasawa, Jpn. J. Appl. Phys., Part 2 33 (1994) L1338.
[8] H. Onishi, Y. Iwasawa, Chem. Phys. Lett. 226 (1994) 111.
[9] H. Onishi, Y. Iwasawa, Surf. Sci. 313 (1994) L783.
[10] H. Onishi, Y. Iwasawa, Surf. Sci. 357 (1996) 773.
[11] C. Y. Nakakura, V. M. Phanse, G. Zheng, G. Bannon, E. I. Altman, K. P. Lee, Rev. Sci. Instrum. 69 (1998) 3251.
[12] B. A. Banse, B. E. Koel, Surf. Sci. 232 (1990) 275.
[13] D. T. Vu, K. A. R. Mitchell, O. L. Warren, P. A. Thiel, Surf. Sci. 318 (1994) 129.
[14] C. Y. Nakakura, G. Zheng, E. I. Altman, Surf. Sci. 401 (1998) 173.
[15] G. Zheng, E. I. Altman, Surf. Sci. 462 (2000) 151.
[16] F. H. Jones, K. Rawlings, J. S. Foord, R. G. Egdell, J. B. Pethica, B. M. R. Wanklyn, S. C. Parker, P. M. Oliver, Surf. Sci. 359 (1996) 107.
[17] R. E. Tanner, E. I. Altman, J. Vac. Sci. Technol. A 19 (2001) 1502.
[18] R. E. Tanner, Y. Liang, E. I. Altman, Surf. Sci. 506 (2002) 251.
[19] R. E. Tanner, P. Meethunkij, E. I. Altman, J. Phys. Chem. B 51 (2000) 12315.
[20] Y. Liang, S. Gan, S. A. Chambers, E. I. Altman, Phys. Rev. B 63 (2001) 235402.
[21] M. Murakami, Y. Matsumoto, K. Nakajima, T. Makino, Y. Segawa, T. Chikyow, P. Ahmet, M. Kawasaki, H. Koinuma, Appl. Phys. Lett. 78 (2001) 2664.
[22] S.A. Chambers, C.M. Wang, S. Thevuthasan, T. Droubay, D.E. McCready, A.S. Lea, V. Shutthanandan, C.F. Windisch, Thin Solid Films 414 (2002) 197.
[23] S. A. Chambers, S. Thevuthasan, R. D. C. Farrow, et al., Appl. Phys. Lett. 79 (2002) 3467.
[24] G. S. Herman, M. R. Sievers, Y. Gao, Phys. Rev. Lett. 84 (2000) 3354.
[25] R. Hengerer, B. Bolliger, M. Erbudak, M. Grätzel, Surf. Sci. 460 (2000) 162.
[26] K. S. Kim, M. A. Barteau, Langmuir 4 (1988) 945.
[27] K. S. Kim, M. A. Barteau, Langmuir 6 (1990) 1485.
[28] K. S. Kim, M. A. Barteau, J. Catal. 125 (1990) 353.
[29] H. Idriss, V. S. Lusvardi, M. A. Barteau, Surf. Sci. 348 (1996) 39.
[30] R. E. Tanner, E. I. Altman, A. Sasahara, H. Onishi, Y. Liang, J. Phys. Chem. B 106 (2002) 8211.
[31] U. Diebold, Surf. Sci. Rep. 48 (2003) 53.
[32] M. Lazzeri, A. Selloni, Phys. Rev. Lett. 87 (2001) 266105.
[33] D. Ciuparu, M. R. Lyubovsky, E. I. Altman, L. D. Pfefferle, A. Datye, Catal. Rev. 44 (2002) 593.
[34] M. Valden, J. Pere, M. Hirismäki, S. Suhonen, M. Pessa, Surf. Sci. 377 (1997) 605.
[35] M. Valden, J. Pere, N. Xiang, M. Pessa, Chem. Phys. Lett. 257 (1996) 289.
[36] G. Zheng, E. I. Altman, Surf. Sci. 462 (2000) 151.
[37] G. Zheng, E. I. Altman, Surf. Sci. 504 (2002) 253.
[38] G. Zheng, E. I. Altman, J. Phys. Chem. B 106 (2002) 1048.
[39] S. -L. Chang, P. A. Thiel, J. Chem. Phys. 88 (1988) 2071.
[40] S. -L. Chang, P. A. Thiel, J. W. Evans, Surf. Sci. 205 (1988) 117.